Direct Numerical Simulation of Axisymmetric Jets

F. F. Grinstein*
Berkeley Research Associates, Inc., Springfield, Virginia
and
E. S. Oran† and J. P. Boris‡
Naval Research Laboratory, Washington, DC

Results are presented from numerical simulations of the evolution of the Kelvin-Helmholtz instability for an unforced, subsonic, compressible, axisymmetric, spatially evolving shear layer. In addition, we study the effect of small, random pressure fluctuations at the nozzle orifice on the growth of the mixing layer. These fluctuations model inflow perturbations in experimental flows arising from turbulence and boundary layers in the nozzle. The finite-difference numerical model used to perform the simulations solves the two-dimensional, time-dependent conservation equations for an ideal fluid using the Flux-Corrected Transport algorithm and time-step-splitting techniques. Although no subgrid turbulence model has been included, the nonlinear properties of the convection algorithm insure that energy in wavelengths smaller than a few computational cells is dissipated. In the absence of perturbations, the calculations indicate that the large-scale development of the unforced jet shear layer has an underlying degree of organization. This is the result of a feedback mechanism in which the shear layer ahead of the nozzle edge is modulated by the far field induced by the mergings downstream, near the end of the potential core of the jet. The studies with random high-frequency perturbations on the inflow velocity show that the perturbations tend to break the temporal correlations between the structures.

Introduction

EXPERIMENTAL investigations in the past decade have shown that large, spanwise coherent structures dominate the entrainment and mixing processes in shear layers.[1-4] Recently, it has become possible to study these structures by direct numerical simulation of their large-scale features. These simulations are an important alternative and supplementary tool in the basic research of the properties of fluid flow transitioning to turbulence. Since a simulation can calculate values for all of the primary flowfield properties as a function of time, statistical information can be obtained about the system through spatial and temporal averages. In addition, parameters of the flow can be easily varied, and the conditions of the calculations are more easily controlled than those in a laboratory experiment.

Numerical studies of coherent structures have used spectral,[5] vortex dynamics,[6] and finite-difference[7-9] techniques. Numerical studies of the evolution of flows similar to those seen in the laboratory experiments have been considered for both two-dimensional planar and axisymmetric shear layers. Previous finite-difference calculations have modeled either temporally developing mixing layers,[7] where it is assumed that the vortex dynamics take place in a relatively compact region of space, or spatially developing layers,[8-10] which correspond more closely to the laboratory experiments.

Previously we performed finite-difference, compressible, spatially developing simulations of planar shear flows, with the objective of investigating asymmetries in mixing[9] and the basic mechanisms involved in the reinitiation of the instabilities.[10] Here we describe finite-difference calculations of the evolution of the Kelvin-Helmholtz instability for a spatially evolving, compressible, axisymmetric freejet. The instabilities sustain themselves through a feedback mechanism in the flow. The evolution and merging of the downstream structures affect the inflowing material upstream, thus triggering the growth and shedding of new vortices.[10] In addition, we study the effect of small, random pressure fluctuations at the nozzle orifice on the growth of the mixing layer. These fluctuations model inflow perturbations in experimental flows arising from turbulence and boundary layers in the nozzle.

Received Nov. 25, 1985; presented as Paper 86-0039 at the AIAA 24th Aerospace Science Meeting, Reno, NV, Jan. 6-9, 1986; revision submitted April 29, 1986. This paper is declared a work of the U.S. Government and is therefore not subject to copyright protection in the United States.

*Research Physicist.
†Senior Scientist, Laboratory for Computational Physics and Fluid Dynamics. Member AIAA.
‡Chief Scientist, Laboratory for Computational Physics and Fluid Dynamics.

Numerical Model

The numerical model used to perform the simulations solves the two-dimensional, time-dependent conservation equations for mass, momentum, and energy for an ideal gas:

$$\frac{\partial \rho}{\partial t} = -\nabla \cdot \rho V \tag{1}$$

$$\frac{\partial (\rho V)}{\partial t} = -\nabla \cdot \rho VV - \nabla P \tag{2}$$

$$\frac{\partial \epsilon}{\partial t} = -\nabla \cdot \epsilon V \cdot V - \nabla \cdot PV \tag{3}$$

where $\epsilon = P/(\gamma - 1) + \frac{1}{2}\rho V^2$ is the internal energy, and V, P, ρ, and γ are the velocity, pressure, mass density, and the ratio of specific heats. The equations are solved using the flux-corrected transport (FCT) algorithm[11] and timestep-splitting techniques. FCT is an explicit finite-difference algorithm that insures that all conserved quantities remain monotonic and positive. FCT modifies the linear properties of a high-order algorithm by adding diffusion during convective transport to prevent dispersive ripples from arising. The added diffusion is subtracted out in an antidiffusion phase of the integration cycle. These processes maintain high-order accuracy without artificial viscosity to stabilize the algorithm. A fourth-order phase-accurate FCT algorithm was used in this work. No subgrid turbulence beyond the natural FCT filtering has been included at this stage. The nonlinear properties of the FCT algorithm insure that energy

in wavelengths smaller than a few computational cells is dissipated. The model is expected to be adequate in describing large-scale features of gas-phase flow for large Reynolds numbers.

Valid inflow and outflow boundary conditions are needed to insure the proper behavior of the fluids near the boundaries and throughout computational domain. However, accurate transparent boundary conditions that provide adequate information about the region outside of the computational domain are very difficult to define for the numerical simulation of compressible subsonic flows. Because of this difficulty, most of the simulations performed until fairly recently involved temporally developing shear layers. Such simulations replace inflow and outflow conditions with periodic boundary conditions and concentrate on the vorticity dynamics in compact regions. A detailed simulation that investigates feedback phenomena must have spatially developing flows and use a model for inflow and outflow boundary conditions.

The calculations presented below use inflow and outflow boundary conditions that have been developed and tested for multidimensional FCT calculations.[9,12] The density and inflow velocity of the jet are specified, and the energy at the inflow guard cells is determined from a zero-slope condition on the pressure:

$$\rho_g = \rho_{\text{inflow}} \tag{4a}$$

$$v_g = v_{\text{inflow}} \tag{4b}$$

$$P_g = P_1 \tag{4c}$$

where P_1 is the pressure at the first inflow cell. This allows the pressure at the inflow to vary in response to disturbances originated by the fluid accelerations downstream and hence allows feedback. Equation (4c) requires the acoustic waves to reflect at the inflow, which is physically reasonable, because the density and velocity at the inflow are fixed. To make a smoother and more realistic transition to the region of interest behind the lip of the nozzle, we have included a portion of the nozzle inside the computational domain. The conditions allow feedback to occur between the fluid accelerations downstream and the inflowing material, thus allowing the instability to evolve naturally in the calculation.

The conditions at the outflow guard cells define the density and velocity through zeroth- and first-order extrapolations, respectively, from the last two cells:

$$\rho_g = \rho_n \tag{5a}$$

$$v_g = 2v_n - v_{n-1} \tag{5b}$$

These are standard conditions (see, e.g., Ref. 13) that are consistent with fixing the inflow velocity of the jet. The energy at the guard cells is defined in terms of the density and velocity given by Eqs. (5a) and (5b) and the pressure defined by

$$P_g = P_n + [(Y_g - Y_n)/(Y_g - Y_j)](P_{\text{amb}} - P_n) \tag{5c}$$

where Y is either the radial or axial coordinate, and the subscript j refers to the trailing edge of the nozzle. Equation (5c) is the result of interpolating between the pressure values at the boundary P_n and at infinity P_{amb}. It enforces a trend in which the pressure gradient vanishes and the pressure equals P_{amb} at infinite distances from the nozzle. The slow relaxation of the pressure toward the known ambient value is necessary because the pressure at the inflow is not specified but calculated from other variables. By giving a reference pressure value, we avoid secular errors in the calculations.

The computational grid was set up initially and held fixed in time. The timesteps were chosen to satisfy the Courant condition. The basic finite-difference grid used 120 cells in the cross-stream (radial) direction and 220 in the streamwise (axial) direction, with the mesh spacings varying in the ranges $0.05 \le \Delta Z \le 0.52$ cm and $0.02 \le \Delta R \le 0.67$ cm. Figure 1 shows a schematic diagram of the grid. The cells are closely spaced in the radial R direction across the shear layer, where the large structures form, and they become farther apart as the distance from the shear layer increases for $R > R_0$. The cell separations in the streamwise direction Z also increase in size as we move away from the trailing edge of the nozzle, located at $R_0 = 0.9$ cm and $Z = Z_0 \approx 1.67$ cm. The cell spacing chosen takes advantage of the fact that the structures merge and grow downstream, so that fewer cells are necessary to keep the resolution the same as that near the nozzle.

The dependence of the results on the boundary conditions, the locations where they were implemented, and the gridding was investigated. As part of the tests, calculations were performed on grids which doubled the resolution of the 220×120 grid on the axial or radial directions, on differently stretched grids, and also on computational domains having inflow plenums with different streamwise extents (e.g., with the inflow at the lip of the nozzle). By comparing the results in the basic 220×120 grid calculation shown in this paper with the calculations in these various other cases, we found that the features we describe below persisted. Furthermore, the agreement with experiments gives confidence that the feedback observed in the simulations are not of numerical origin.

Unforced Axisymmetric Jet

The system studied is a high-speed freejet containing a mixture of molecular hydrogen and nitrogen emerging into a quiescent background mixture of molecular oxygen and nitrogen. The jet-to-background density ratio was 0.67, and the system was initially at a uniform temperature (298 K) and pressure (1 atm). A step function at $R = R_0$ was used as the initial axial velocity profile. The jet was subsonic, with Mach number 0.57 and a corresponding velocity of 2.0×10^4 cm/s. Figure 2 is a schematic diagram of the flow configuration. The instabilities were initiated by a small cross-stream pressure gradient. This occurred only at the very beginning of the calculation and perturbed the thin vorticity layer just ahead of the nozzle edge. As the calculation evolves, the disturbance moves downstream and generates the transverse flows that trigger the Kelvin-Helmholtz instability. Previously, we considered initial sinusoidal perturbations along the shear interface.[12] The approach used in this paper to initiate the instability was also used in the simulations of planar shear flows.[9,10] Morkovin (private communication) has pointed out that this initiation is closely analogous to using a weak, spark-produced, pressure N-wave perturbation[14] during the first few integration cycles.

Typical features of the early stages of the flow are shown in the sequence of isovorticity contours in Fig. 3. The vortex rings are the result of the nonlinear evolution of the instability. The rings emerge at an essentially fixed distance from the nozzle edge, somewhat less than 1 diam, $D = 2R_0$, at $z = (Z - Z_0)/D \approx 0.7$. The newly formed structures move along the interface, interact with each other, and thereby spread the vorticity until the potential core region disap-

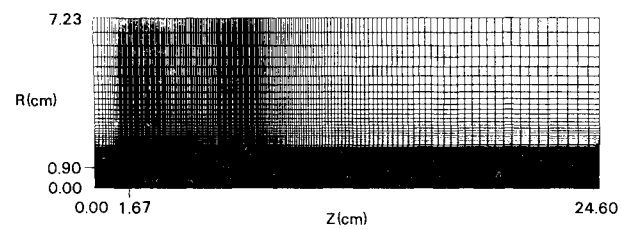

Fig. 1 Schematic diagram of the 220×120 computational grid.

pears, at approximately $z=5$. Upstream of this location, the structures are displaced vertically by a low-frequency modulation of the shear layer. When this modulation is appropriately phased with the locations of the structures, three structures merge into a larger structure in half of the modulation cycle. Since the jet is unforced, the low-frequency modulation must be caused by the pressure field induced by the larger, downstream structures.

In previous papers dealing with planar, unforced shear flows,[9,10] we noted feedback between the downstream events and the inflowing streams. Because of the way in which we initialized the simulations, i.e., with a transient perturbation just behind the edge of the splitter plate or the nozzle, we could trace the evolution of the flow and observe the effect of the downstream events on the upstream shear layer. We were able to identify a feedback process responsible for the reinitiation of the instabilities, and that leads to new vortex roll-ups near the trailing edge of the splitter plate. The feedback process operates through the velocity field induced by the nearby flowfield. In addition, the fluid accelerations involved in the downstream vortex mergings induced vertical displacements of the upstream vortices. This, in turn, triggered further mergings and indicated that there was also a longer-range feedback effect strongly affecting the growth of the mixing layer. Both the short-range and long-range effects we identified are present in the simulations that we are discussing.

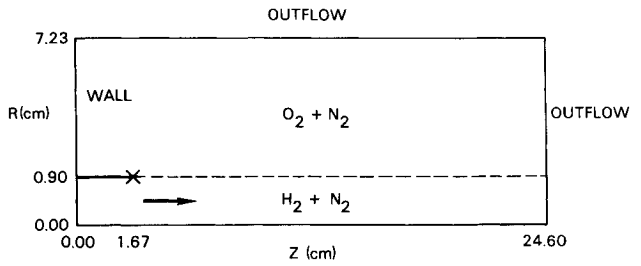

Fig. 2 Flow configuration for the axisymmetric jet simulation. The trailing edge of the nozzle is located at x.

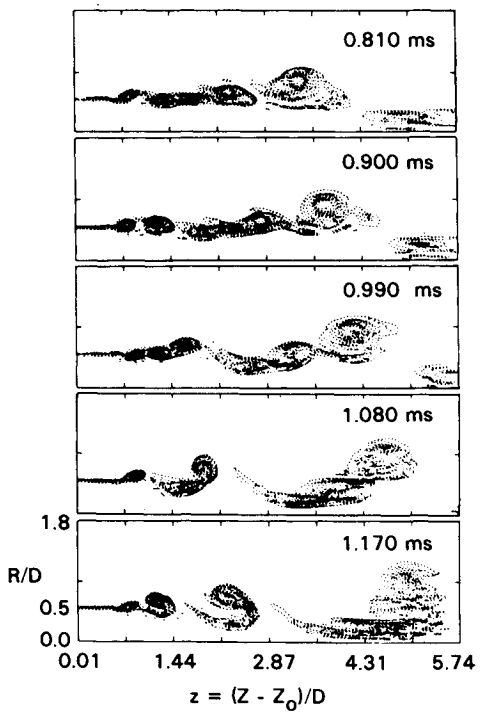

Fig. 3 Initial stages in the flow development.

As the effect of the downstream events on the inflowing fluid becomes important, there is an interaction between the basic instability mechanism at the shear layer and the feedback mechanism. The flow pattern subsequently becomes different from that at the initial stages in the flow development, which was dominated by the shear layer instability. A strong spatial and temporal correlation between the mergings is set up. The effects of this correlation can be seen in the last panel of Fig. 3, which shows a pattern in the distribution of the locations of vortex merging which subsequently becomes essentially fixed.

Frames at much later times in the development of the flow can be seen in Fig. 4. A noticeable feature of this sequence of frames is a regularly repeating spatial pattern, in which vortex shedding and vortex pairing occur at essentially fixed locations. Based on the results of the calculations for these later times, we have performed a spectral analysis of the axial velocity fluctuations. In the sequence of panels in Fig. 5, we show the spectra at various axial locations along the centerline of the shear layer ($R=R_0$). These spectra are given in terms of the normalized Strouhal frequency $St=2\pi f\theta_0/v_0$, where θ_0 and v_0 are the initial momentum thickness of the shear layer and the jet velocity, respectively. The shear layer thickness was taken as $\theta_0=\Delta R=0.02$ cm, where ΔR is the size of a radial cell in the region of the shear layer. This is a natural choice for θ_0 because the step of the initial velocity profile is defined within ΔR.

Figure 5a, corresponding to a location very close to the nozzle exit, shows peaks at the frequencies $St_0\approx 0.100$, $St_1\approx 0.050$, $St_2\approx 0.025$, $St_+\approx 0.125$, and $St_-\approx 0.075$. Here, St_0 is associated with the shear-layer instability frequency. This value is in good quantitative agreement with the predictions of linear inviscid instability theory[15] based on v_0, R_0, and θ_0. In addition, the modulation of the initial shear layer with $St_1\approx St_0/2$ and $St_2\approx St_0/4$ is associated with the first and second subharmonic, and $St\pm\approx(St_0\pm St_2)$ result from the nonlinear interaction between the shear-layer instability and the feedback process. The low-frequency modulation is dominated by the peak at St_2, which, in terms of the Strouhal number based on the jet diameter $St_D=fD/v_0$, is associated with $St_D\approx 0.36$. This is within the range $0.2\leq St_D\leq 0.5$, in which the frequency of the largest scales of an unforced subsonic jet, the preferred jet mode, is

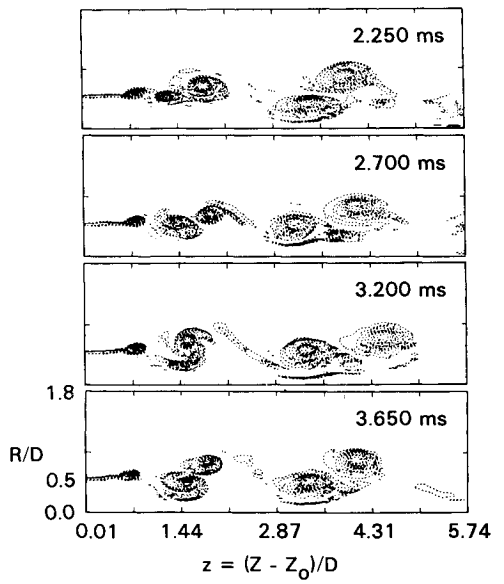

Fig. 4 Regularity and spatial coherence of the flow development for the unforced jet.

known to lie.[16,17] As we move downstream, the high-frequency amplitudes tend to diminish, as can be expected. In Figs. 5b and 5c, the amplitude for the natural shear-layer mode St_0 progressively diminishes as the amplitudes for frequencies in the neighborhood of its first subharmonic St_1 become more important. Thus, Figs. 5b and 5c correspond to locations at the beginning and concluding stages of a first merging associated with St_1. Similarly, Figs. 5d and 5e correspond to locations where second (associated with St_2) and third (associated with $St_3 \approx St_0/8$) mergings are taking place.

Flow visualization, as shown in Fig. 6, allows us to determine the locations of vortex pairing. These locations are defined to be those places where the centers of the two vortices are vertically aligned and where the amplitudes of the corresponding subharmonics are expected to saturate.[18] Through the sequence of panels in Fig. 6, we see that the locations of the first, second, and third mergings are at about $z_1 \approx 1.0$, $z_2 \approx 1.9$, and $z_3 \approx 4.4$, respectively. There is a close agreement between the merging locations obtained from the flow visualization and the results of the spectral analysis. The end of the potential core lies between the locations of the second and third mergings. Thus, the low-frequency peak in the power spectra close to the nozzle of the jet, corresponding to the dominant modulation of the oscillations, is associated with the vortex passage frequency at the end of the potential core. This is as observed in the experiments by Laufer and Monkewitz.[19]

In Fig. 7 we have shown the distribution of merging locations and compared them with those in the experiments by Kibens with weakly excited circular jets.[16] The distributions are in qualitative agreement and show the same linear trend.

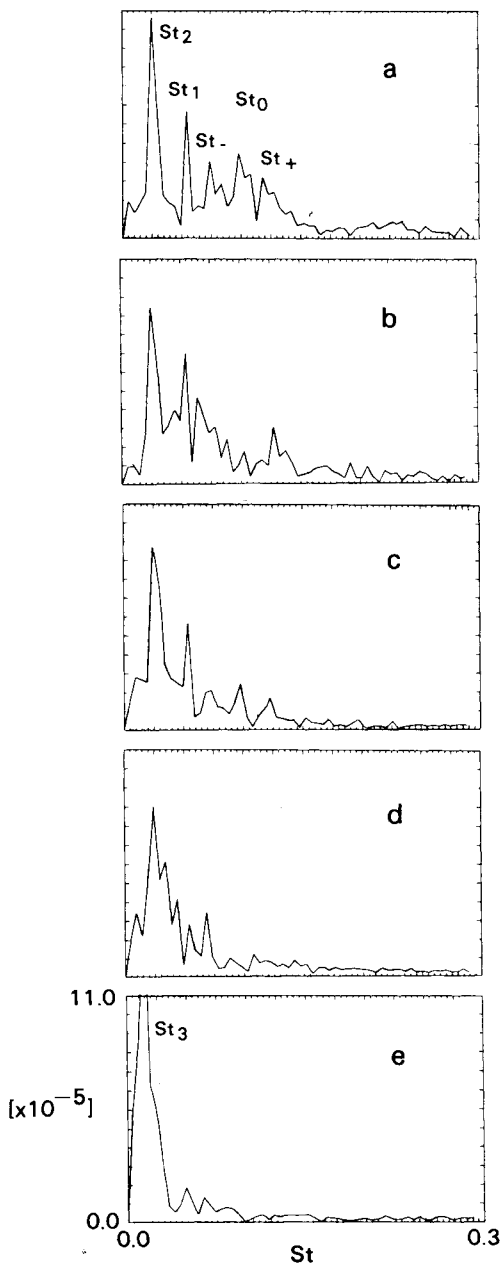

Fig. 5 Spectra of the axial velocity fluctuations at $R/D = 0.5$ and various axial locations: a) $z = 0.40$; b) $z = 0.71$; c) $z = 1.04$; d) $z = 1.98$; e) $z = 4.32$. The vertical scale is linear and has arbitrary units.

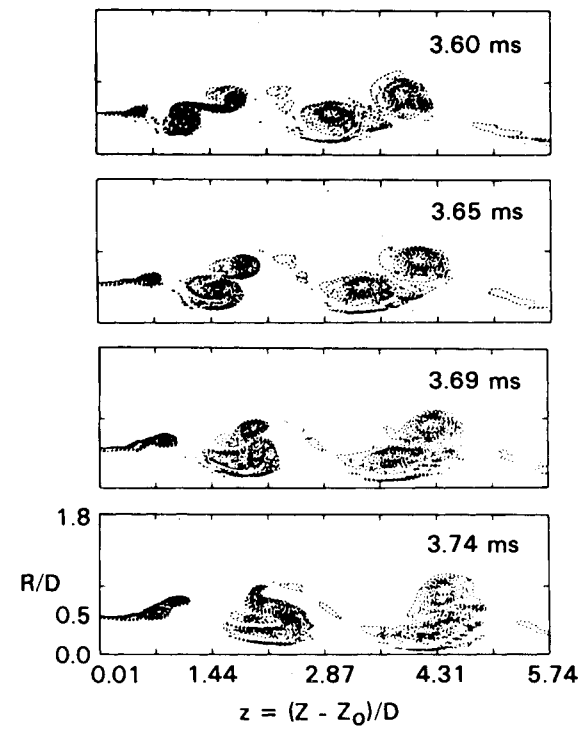

Fig. 6 Flow visualization showing detailed vortex mergings.

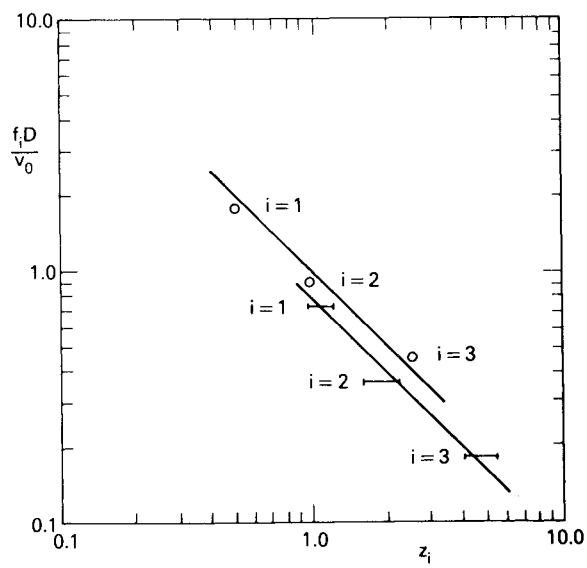

Fig. 7 Merging locations. o: Kibens, Ref. 12; |—|: intervals where the locations are distributed in the present simulations; ——: feedback formula, Eq. (6), for $N = 2$.

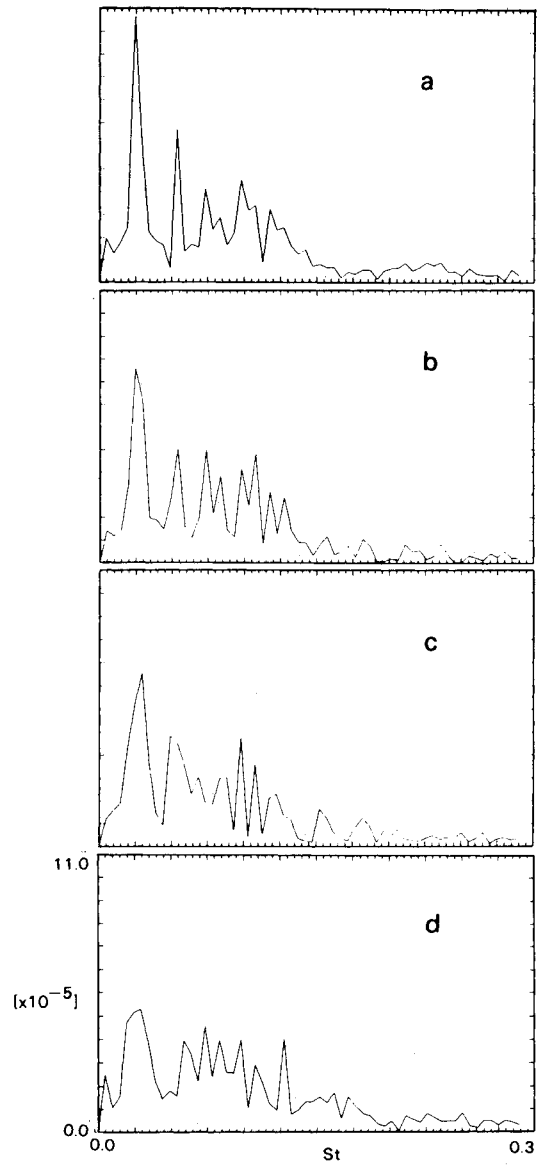

Fig. 8 Spectra of the axial velocity fluctuations at $R/D=0.5$ and $z=0.40$, with and without random inflow perturbations: a) unperturbed; b) fluctuation level 0.1%; c) 1%; and d) 5%. The vertical scale is linear and has arbitrary units.

As a consequence, a feedback formula, such as Laufer and Monkewitz used to fit the experimental merging locations,[19] is expected to fit the distribution obtained in the present simulations. This feedback formula[19,20] depends on the superposition of the processes of convection of the instabilities downstream toward the merging location and the propagation upstream of acoustic waves caused by the merging. The locations of vortex merging are defined by a resonance condition

$$\frac{f_i D}{v_0} z_i \left[\frac{v_0}{v_c} + \frac{v_0}{a}\right] = N \tag{6}$$

where $f_i = f_0/2^i$ and z_i are the frequency and location of the ith pairing, $v_c = v_0/2$ is the convection velocity, a is the velocity of sound, and N is a positive integer. The formula requires that the sum of the time for convection from the lip of the nozzle to the merging location and the time for acoustic propagation upstream, back to the nozzle, be an integer multiple of the merging period. The convection and sound velocity are assumed to be effectively constant in the derivation of the formula. The generalization is, however, straightforward. Both the data of Kibens and those obtained in our simulations can be reasonably fit with Eq. (6) for $N=2$, as shown in Fig. 7. The downward shift of simulation data relative to the experimental data can be understood from Eq. (6) as an effect of compressibility due to the considerably larger Mach number $M=v_0/a$ in the flow conditions of the simulations. These agreements give a consistency check of both Eq. (6) and the results of the simulations and show the presence of feedback phenomena.

Effect of Random Inflow Perturbations

We have also simulated the effects of high-frequency random perturbations in the inflowing jetstream. Such fluctuations in the experimental conditions in the laboratory are due to turbulence and boundary layers in the nozzle. In the calculations, the fluctuations are modeled by replacing the streamwise velocity U at the inflow (i.e., for $Z=0$ cm, $R \le R_0$) with $U(1+p)$, where $p=p(R,t)$ is the perturbing term. This term is defined by a sine Fourier series in the variable R, with R_0 the largest wavelength:

$$p(R,t) = \frac{1}{M} \sum_{m=1}^{M} p_m^0 \delta_m(t) \sin\left(\frac{2\pi m R}{R_0} + \phi m\right) \tag{7}$$

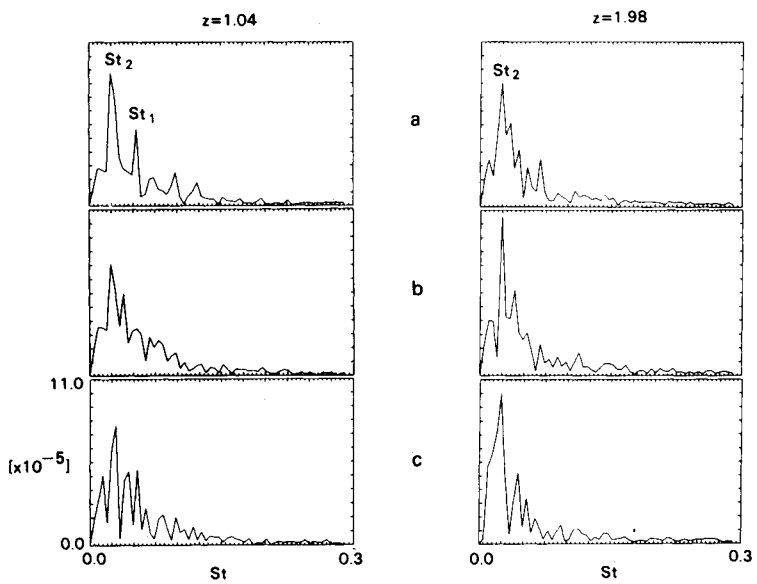

Fig. 9 Spectra of the axial velocity fluctuations at $R/D=0.5$ and at locations of the first and second mergings for the unperturbed case, at $z=0.71$ and $z=1.98$, respectively, as a function of the inflow fluctuation level: a) unperturbed; b) fluctuation level 0.1%; c) 1%. The vertical scale is linear and has arbitary units.

where $\delta_m(t)$ is a time-dependent amplitude defined by

$$\begin{aligned}\delta_m(t) &= 2(t-t_{0m})/\delta t_m && \text{if } t_{0m} \le t \le t_{0m}+\delta t_m/2\\ &= 2(t_{0m}-t)/\delta t_m + 2 && \text{if } t_{0m}+\delta t_m/2 \le t \le t_{0m}+\delta t_m\\ &= 0 && \text{otherwise}\end{aligned}$$

In this way, each perturbation term in Eq. (7) varies between zero and a maximum value of no more than a fraction p_m^0/M of the inflow jet velocity. The duration δt_m, the maximum value p_m^0 of the amplitude, and the phases $\phi_m (0 \le \phi_m \le 2\pi)$ of the terms in the Fourier series are randomly generated numbers.

A calculation was performed which restarted the program at time $t = 2.52$ ms of the unperturbed calculation, but with inflow fluctuations now included. The series in Eq. (7) was truncated at $M = 4$. Thus, only fluctuations of wavelength R_0, $R_0/2$, $R_0/3$, and $R_0/4$ were included, with durations δ_m in the range of 5–12.5 μs (20–50 time steps).

Because of the changes in the frequency content of the velocity field, the previously noted regularity in the flow pattern was lost in spite of the relatively small amplitude of the fluctuations. This can be seen by comparing the spectral distributions obtained in this perturbed case with those for the unperturbed case discussed previously. Figures 8a–8d show the spectral distributions near the lip of the nozzle and at the center of the shear layer for mean perturbation levels of 0,0.1, 1, and 5%. The figure shows that increasing the perturbation level causes the peaks to broaden, and new high-frequency peaks are now present. Figure 9 is a similar comparison of spectral distributions at the locations of the first two mergings for the unperturbed case. The changes in the spectra are significant even in the weakest (0.1% level) perturbed case. This indicates that more incoherent mergings now occur, and the merging locations are progressively less well defined as the perturbation level increases.

Summary and Conclusions

We have presented results from finite-difference numerical simulations of the evolution of the Kelvin-Helmholtz instability for a subsonic, compressible, axisymmetric, spatially evolving shear layer. We have found that, in spite of the two-dimensional restriction of the simulations, there is general agreement between the calculated and experimentally observed distribution of vortex merging locations. In addition, there is agreement between the calculations and the experiments on the effect of the fluid accelerations at the end of the potential core on the upstream shear layer. This effect appears as a dominant low-frequency peak characterizing the modulation of the oscillations in the shear layer just ahead of the nozzle. Such a peak is observed in the experiments by Laufer and Monkewitz,[19] and in our calculations it corresponds to the frequency St_2 of the second merging, which occurs very close and upstream of the end of the potential core.

The calculations show that the large-scale development of the unforced jet shear layer has an underlying degree of organization. This organization is the result of a feedback process in which the shear layer ahead of the nozzle edge is modulated by the flowfield induced by the mergings downstream, near the end of the potential core of the jet. The fact that the distribution of merging locations was essentially fixed and in agreement with the predictions of the feedback formula is evidence for this feedback. We also observed the presence of this feedback mechanism in our simulations of planar shear flows.[9,10] Note, however, that this is an idealized case of an axisymmetric flow with no boundary layers or small-scale inflow turbulence.

The dominant frequencies in the unforced flow depend on the initial shear layer thickness and the jet diameter, the two length-scales of the jet. These scales are associated with the two basic instabilities in the jet, the jet shear layer instability and the jet column instability. These instabilities determine the high- and low-frequency natural modes of the jet, respectively. The spectral analysis of the axial velocity fluctuations at the centerline of the shear layer, just ahead of the nozzle edge, shows a sequence of peaks separated by an interval approximately equal to $St_0/4$. These peaks correspond to the subharmonics of the jet shear layer instability frequency St_0 and to the nonlinear interactions between the modes associated with them. The Strouhal number for the preferred jet mode, $St_D = (f_0/4)D/v_0 \approx 0.36$, is in good agreement with the experimental values for subsonic jets. Moreover, the value for St_0 was consistent with the predictions of linear inviscid instability theory.

The studies with random high-frequency perturbations on the inflow velocity show that such perturbations tend to break the organized jet shear layer and hence the temporal coherence between the structures. By generating more incoherent mergings, the fluctuations tend to destroy the regularity of the idealized, unforced two-dimensional case.

Acknowledgments

We would like to acknowledge useful discussions with Dr. K. Kailasanath. We also thank Professor M. V. Morkovin for bringing to our attention the work by L. J. Poldervaart et al. reviewed in Ref. 15. This work was sponsored by the Mechanics Division of the Office of Naval Research and by the Naval Research Laboratory.

References

[1]Winant, C. D. and Browand, F. K., "Vortex Pairing, the Mechanism of Turbulent Mixing-Layer Growth at Moderate Reynolds Number," *Journal of Fluid Mechanics,* Vol. 63, 1974, pp. 237–255.

[2]Brown, G. and Roshko, A., "On Density Effects and Large Structure in Turbulent Mixing Layers," *Journal of Fluid Mechanics,* Vol. 64, 1974, pp. 775–816.

[3]Browand, F. K. and Ho, C. M., "The Mixing Layer: An Example of Quasi Two-Dimensional Turbulence," *Journal de Mécanique Théorique et Apliquée,* Numéro spécial, 1983, pp. 99–120.

[4]Hussain, A.K.M.F., "Coherent Structures—Reality and Myth," *Physics of FLuids,* Vol. 26, 1983, pp. 2816–2850.

[5]Riley, J. J. and Metcalfe, R. W., "Direct Numerical Simulation of a Perturbed Turbulent Mixing Layer," AIAA Paper 80-0274, 1980.

[6]Ghoniem, A. F. and Ng, K. K., "Effect of Harmonic Modulation on Rates of Entrainment in a Confined Shear Layer," AIAA Paper 86-0056, 1986.

[7]Corcos, G. M. and Sherman, F. S., "The Mixing Layer: Deterministic Models of a Turbulent Flow. Part 1. Introduction and the Two-Dimensional Flow," *Journal of Fluid Mechanics,* Vol. 139, 1984, pp. 29–65.

[8]Davis, R. W. and Moore, E. F., "A Numerical Study of Vortex Merging in Mixing Layers," *Journal of Physics and Fluids,* Vol. 28, 1985, pp. 1626–1635.

[9]Grinstein, F. F., Oran, E. S. and Boris, J. P., "Numerical Simulations of Asymmetric Mixing in Planar Shear Flows," *Journal of Fluid Mechanics,* Vol. 165, 1986, pp. 201–220.

[10]Grinstein, F. F., Oran, E. S. and Boris, J. P., "Numerical Simulation of Unforced Spatially-Developing Mixing Layers," submitted to *Journal of Fluid Mechanics.*

[11]Boris, J. P. and Book, D., "Solution of Continuity Equations by the Method of Flux Corrected Transport," *Methods in Computational Physics,* Vol. 16, Ch. 11, Academic Press, 1976; also, Boris, J. P., NRL Memorandum Rept. 327, Naval Research Laboratory, Washington, DC, 1976.

[12]Boris, J. P., Oran, E. S., Gardner, J. H., Grinstein, F. F. and Oswald, C. E., "Direct Simulations of Spatially Evolving Compressible Turbuelnce—Techniques adn Results," *Ninth International*

Conference on Numerical Methods in Fluid Mechanics, edited by Soubbaramayer and J. P. Boujot, Springer, New York, 1985, pp. 98–102.

[13]Yee, H. C., "Numerical Approximation of Boundary Conditions with Applications to Inviscid Equations of Gas Dynamics," NASA TM 81265, 1981.

[14]Ffowcs Williams, J. E., "Film Reviews," *Journal of Fluid Mechanics,* Vol. 78, 1976, pp. 859–860.

[15]Michalke, A., "Instability of Compressible Circular Free Jet with Consideration of the Influence of the Jet Boundary Layer Thickness," NASA TM 75190, 1977; also, Michalke, A. and Hermann, G., "On the Inviscid Instability of a Circular Jet with External Flow," *Journal of Fluid Mechanics,* Vol. 114, 1982, pp. 343–359.

[16]Kibens, V., "Discrete Noise Spectrum Generated by an Acoustically Excited Jet," *AIAA Journal,* Vol. 18, 1979, pp. 434–441.

[17]Hussain, A.K.M.F. and Zaman, K. B. M. Q., "The 'Preferred Mode' of the Axisymmetric Jet," *Journal of Fluid Mechanics,* Vol. 110, 1981, pp. 39–71.

[18]Ho, C. M. and Huang, L. S., "Subharmonics and Vortex Merging in Mixing Layers," *Journal of Fluid Mechanics,* Vol. 119, 1982, pp. 443–473.

[19]Laufer, J. and Monkewitz, P.A., "On Turbulent Jet Flows: A New Perspective," AIAA Paper 80-0962, 1980.

[20]Ho, C. M. and Nosseir, N.S., "Dynamics of an Impinging Jet. Part 1. The Feedback Phenomenon," *Journal of Fluid Mechanics,* Vol. 105, 1981, pp. 119–142.